Kink Band Instability in Layered Structures

M. Ahmer Wadee[⋆], G. W. Hunt[†], and M. A. Peletier[‡]

[⋆]*Department of Civil & Environmental Engineering,*
Imperial College of Science, Technology & Medicine, London SW7 2AZ, UK.
Email: a.wadee@imperial.ac.uk

[†]*Centre for Nonlinear Mechanics, University of Bath, Bath BA2 7AY, UK.*
Email: g.w.hunt@bath.ac.uk

[‡]*Centrum voor Wiskunde en Informatica, Amsterdam, The Netherlands.*
Email: mark.peletier@cwi.nl

Keywords

(A) Kink Banding; (B) Layered Material; Structures; (C) Energy Methods; Stability and Bifurcation

Abstract

A recent two-dimensional prototype model for the initiation of kink banding in compressed layered structures is extended to embrace the two propagation mechanisms of band broadening and band progression. As well as interlayer friction, overburden pressure and layer bending energy, the characteristics of transverse layer compressibility and foundation stiffness are now included. Experiments on constrained layers of paper show good agreement with the predictions of angle of orientation, kink band width and post-kink load-deflection response obtained from the model.

1 Introduction

Kink banding is a phenomenon seen on a variety of scales across the physical sciences. It should be considered as a potential failure mode for any layered or fibrous material, held together by external pressure or some form of internal

"glue", and subjected to layer-parallel compression. Examples can be found in the deformation of geological strata (Anderson, 1964; Hobbs *et al.*, 1976; Price & Cosgrove, 1990), wood and fibre composites (Kyriakides *et al.*, 1995; Reid & Peng, 1997; Fleck, 1997; Hull & Clyne, 1996; Byskov *et al.*, 2002; Vogler & Kyriakides, 2001), and internally in wire and fibre ropes (Hobbs *et al.*, 2000). There have been many attempts to reproduce kink banding theoretically, from early mechanical models (Rosen, 1965; Argon, 1972), to more sophisticated formulations coming from both continuum mechanics (Budiansky, 1983) and numerical perspectives (Vogler *et al.*, 2001). Notable work on layered structures include the theoretical models of Johnson (1995), and the experiments of Ghosh (1968).

Perhaps because composite materials have had such a high profile, most formulations to date have been aimed at fibrous rather than layered structures. Extra problems are then encountered in the modelling process. First, although two dimensional models are commonly employed (Budiansky *et al.*, 1998), modelling into the third dimension adds a significant extra component. It necessarily involves a mix of fibres and either voids or matrix material, and usually has to be handled by some kind of smeared approximation. Secondly, failure is likely to be governed by plastic shear in the matrix material (Fleck, 1997), and this is considerably less easy to measure or control than the combination of overburden pressure and friction considered here.

The formulation follows naturally from earlier work (Hunt *et al.*, 2000; Hunt *et al.*, 2001), with a shift of emphasis from initial instability to subsequent propagation. The motivation is found in structural geology, specifically in the formation of *kink bands* and related *chevron folding* in compressed sedimentary rocks, as seen for example in the exposed cliff face at Millook Haven in Cornwall, just south of Bude. Insight into such mechanisms can be obtained from laboratory experiments on layers of paper constrained by transversely-applied *overburden pressure* and compressed in one of the layer-parallel directions in a loading device. The inclusion of transverse compressibility has added a significant new component to the formulation; the suggestion is made for instance, that release of the initial compression caused by the overburden pressure is instrumental in selecting the orientation of the band across the specimen.

For comparison with experiments, quantitative measures of the coefficient of friction, overburden pressure and compressive load are easy to obtain. More difficult is the extra resistance to band formation coming from the stiffness of the supporting foundation, but this is usefully inferred from the experimental transverse load response. The bending energy incorporated in the layers is again difficult to measure; bands form with near-straight limbs and near-sharp corners, and the curvature of the corner is chosen as a compromise between work done in bending and against overburden pressure. A tailored "corner analysis", based on minimizing the energy contribution of this compromise,

allows the distributed corner energy to be replaced with an equivalent rotational spring. Experimental and theoretical loading curves are then found to agree well over the full loading range.

The paper starts with a description of the loading history of a typical experiment, involving both the initial formation and subsequent propagation of kink bands. This is followed by identification of the significant components of either energy or pseudo-energy (Hunt *et al.*, 2000) that make up the full nonlinear potential function. The experimental response has two distinct phases, instability and propagation, and each is fully reflected in the nonlinear response that follows from the potential energy description. Both kink band rotation and kink band width are included as degrees of freedom, and two different forms of propagation are thus identified, band broadening and band progression. At the point of instability, there is a sudden appearance of a kink band of non-zero width, which broadens under increasing load until formation of a second band, then a third and so on, with progression continuing as new bands form in zig-zag fashion along the length. The body of the paper is devoted to extensions to the mechanical model, and it closes with comparison between the resulting predictions and a few simple experiments.

2 A typical experiment

The following set of experiments was conducted in the Department of Civil and Environmental Engineering at Imperial College London. Layers of A4 size paper (210 mm $\times$ 297 mm) or smaller were held together transversely under a rigid screw device, and then compressed in one of the layer-parallel directions by a second loading system which applied end-shortening at constant rate over a portion of the available layers, as shown in Fig. 1. A photograph of the loading detail and resulting deformation pattern is shown in Fig. 2, the superimposed lines having been added to enable measurement of the orientation angle β. Load cells were used to record both transverse and in-plane loads at one second intervals, and an in-plane transducer registered the corresponding displacement of the in-plane load. Output from a typical experiment is shown in Fig. 3.

A typical loading sequence is as follows. First, an overburden pressure is applied via the transverse screw jack, following which the constraining plates are rigidly held in position. After an initial axial movement to take up the load, the in-plane response follows a near-linear path (A to B), ended by a sudden instability (often accompanied by an audible bang) at B as the first kink band forms. Usually, but not always, this occurs at the loaded end of the sample. The load instantly drops to C, the apparent slope from B to C being a consequence of the time stepping process. A small increase in load

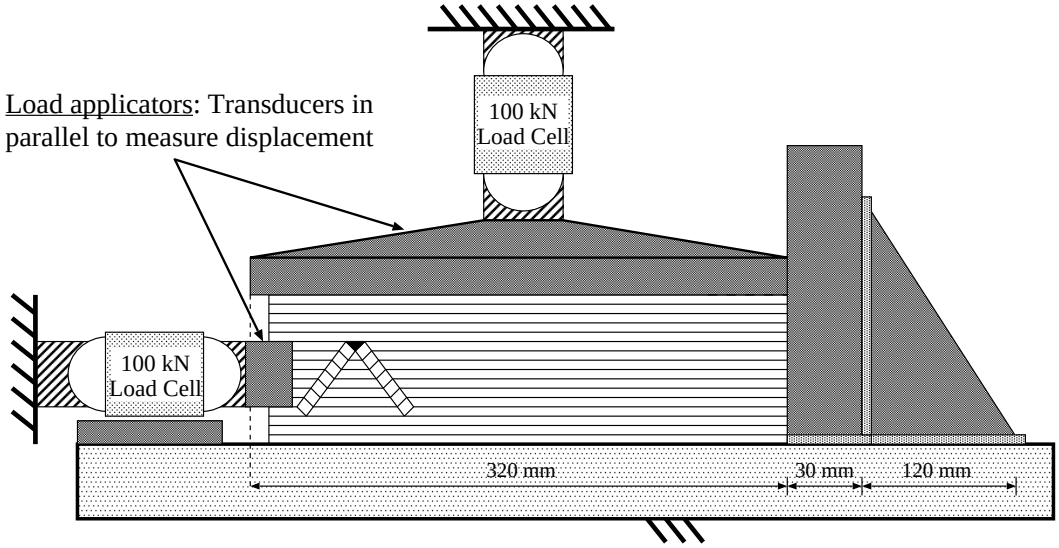

Fig. 1. Schematic side elevation of the experimental rig. Displacment control via two screw jacks can be applied both axially and transversely. The rig can accommodate paper of size A4 (210 mm × 297 mm) and a sample height of 150 mm.

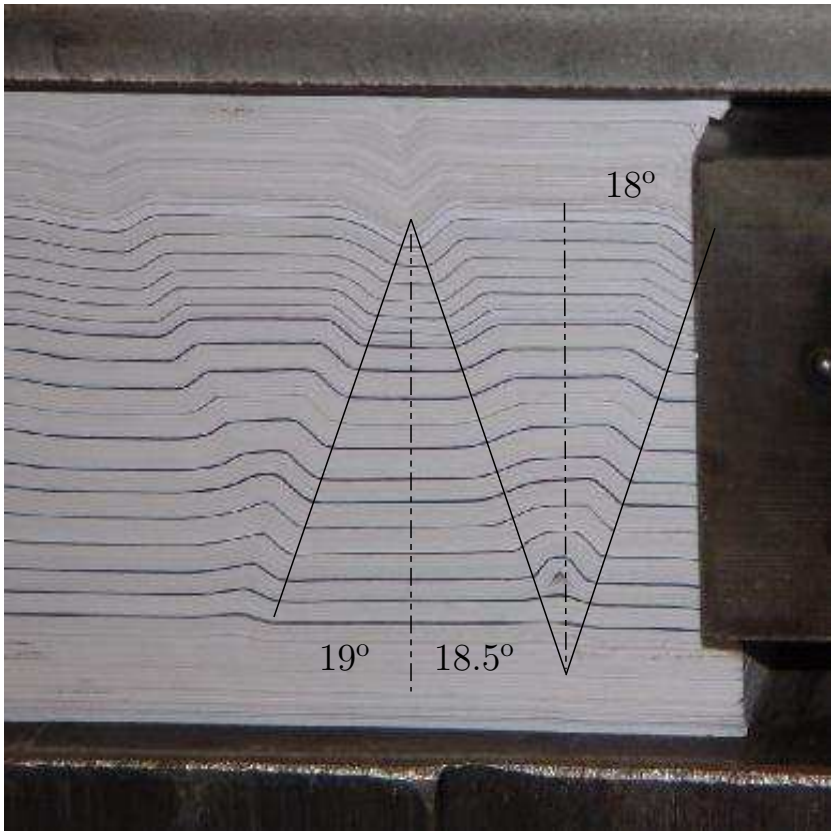

Fig. 2. Deformation under compression of approximately 625 sheets of paper from a sample of 800.

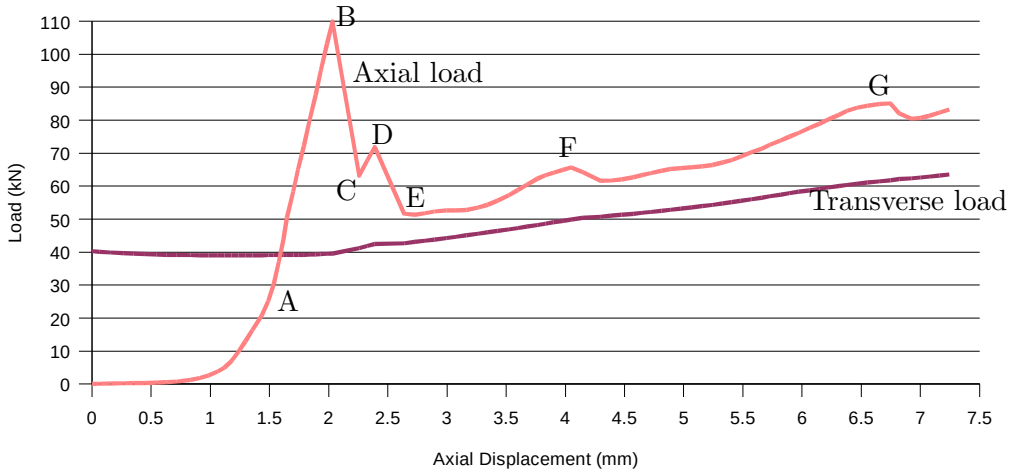

Fig. 3. Output of axial and transverse compressive forces, plotted against axial end shortening.

to D is then terminated by a second drop in load (to E) as the second band forms. Third and fourth bands form in a similar way at points F and G, each being accompanied by a small drop in load after a period of restabilization. Meanwhile, the transverse load remains nearly constant until the first band forms, and increases in near-linear fashion thereafter.

3 Model Characteristics

The formulation used here is developed from earlier models of Hunt *et al.* (2000; 2001), with the important added ingredient of transverse compressibility. A kink band is assumed to be made from straight limbs and sharp corners, as shown in Fig. 4, with the band width b allowed to vary and each layer being of thickness t. Bending energy in each layer is concentrated into two rotational elastic springs of stiffness c at each end of the inclined portion, and the layers are offset relative to one another by the *orientation angle* β as shown in Fig. 4(a). In-line springs k are introduced to provide the undeflected (fundamental) state with a linear elastic response, the overburden pressure is q, and the coefficient of friction between layers is μ. Poisson's ratio effects were assessed and were deemed to be insignificant.

The system has three degrees of freedom, angle of rotation α, band width b and compression of the in-line springs δ. In the present formulation, β is fixed a priori by the transverse compressibility between the layers. This differs from our earlier models, where thickness t was assumed to remain constant and β was either taken as zero, or linked to α by the relation $\alpha = 2\beta$. The $\beta = 0$ (vertical stack) model was unrealistic in that it opened against overburden pressure (Hunt *et al.*, 2000). The second (inclined stack) model managed to eliminate void formation, but at the expense of allowing β to vary; the band

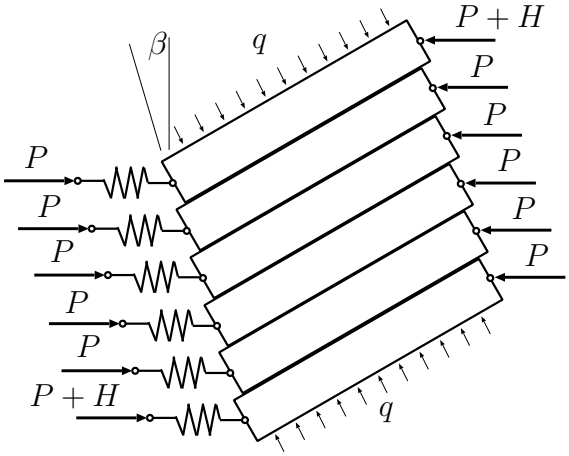

(a)

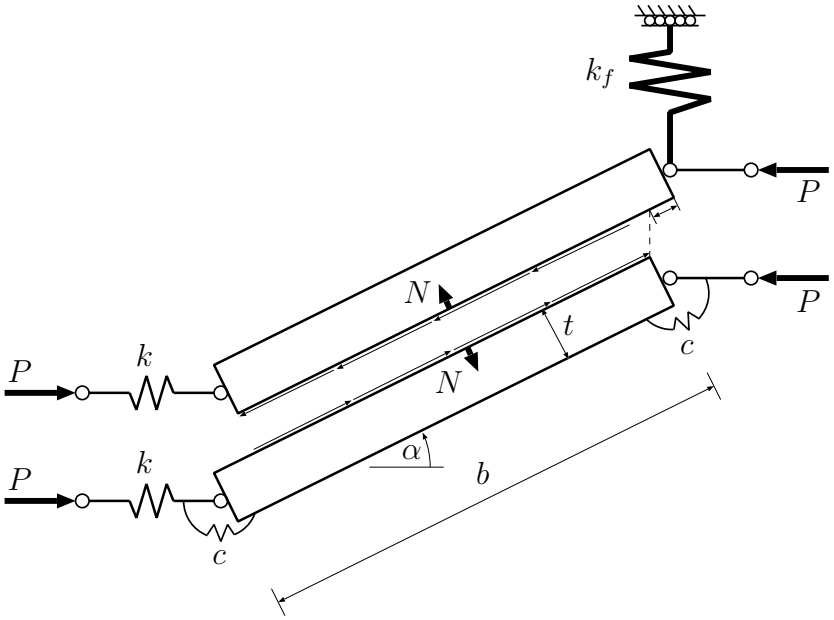

(b)

Fig. 4. (a) Stack of blocks of thickness t at the orientation angle β to the vertical. (b) Representative two-layer section, showing the band width b with single layer contributions to the bending stiffness c (lower layer) and the "foundation" stiffness k_f (upper layer).

would then rotate as α developed from zero, an effect not seen experimentally.

Fig. 5 demonstrates that, if transverse compressibility is allowed, both problems can be avoided: β can remain constant without creating voids. As α grows under constant β, there is an initial dilation within the band, followed by compression and eventual lockup. Maximum dilation occurs at $\alpha = \beta$,

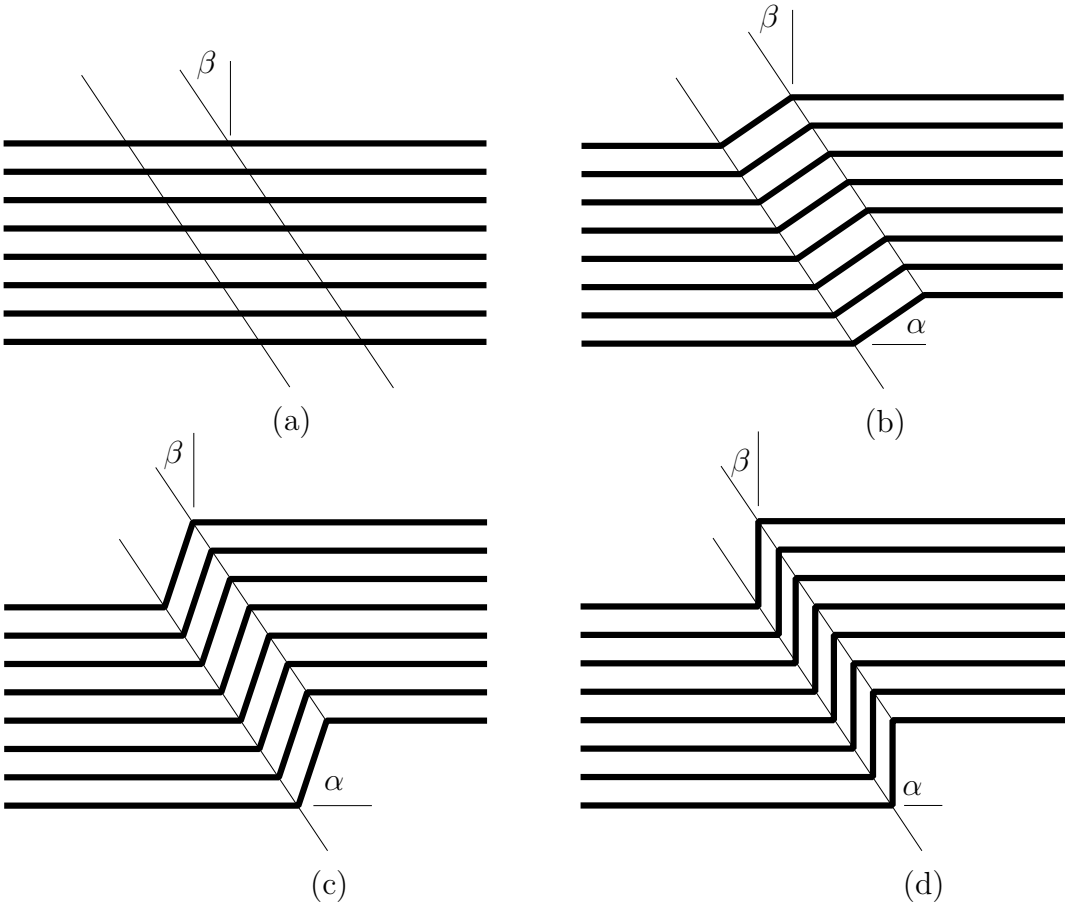

Fig. 5. Kink band formation at constant β. (a) Flat layers under transverse compression. (b) Maximum dilation found at $\alpha = \beta$. (c) Equal thicknesses found at $\alpha = 2\beta$. (d) Lockup at $\alpha > 2\beta$.

and this is taken as responsible for fixing β. By assuming that the transverse stress in the band drops exactly to zero in this state, the work done against friction is naturally minimized. The geometry of Fig. 6 shows both the transverse compression and the slip for two layers of initial (stress-free) thickness t, rotating about fixed pin positions. The thickness is then $t\cos\beta$ at $\alpha = 0$, with a corresponding transverse strain ϵ,

$$\epsilon = 1 - \cos\beta. \tag{1}$$

A typical experimental response of transverse load against its corresponding deflection is shown here in Fig. 7. For the given dimensions, an initial transverse load of 40 kN is seen to produce a transverse strain of about 3.8%. According to the above mechanism, this predicts an orientation angle of $\beta = \arccos(1-0.038) \approx 16°$, which is close to that found experimentally (see Fig. 2). Research groups studying failure of laminated composite materials (Budiansky *et al.*, 1998; Vogler *et al.*, 2001) have also found that the kink band orientation β is sensitive to the layer dilatancy. However, they have been unable to make the sort of accurate comparisons between theory and

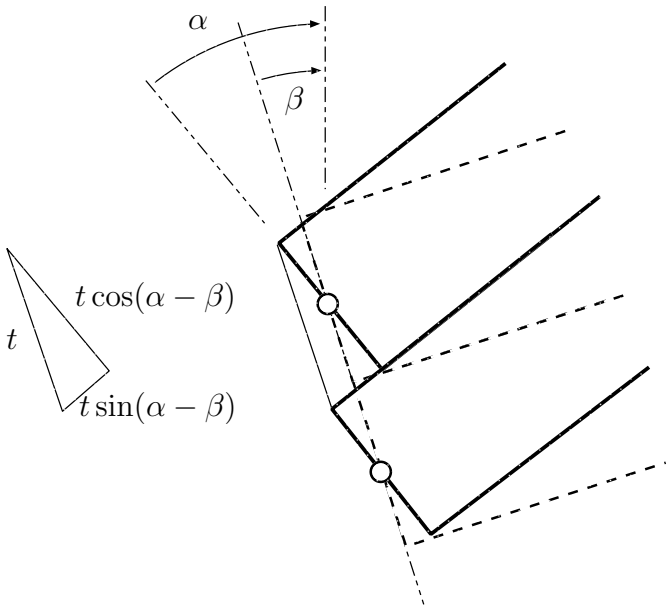

Fig. 6. Thickness change and slip in compressible layers that are of thickness t when $\alpha = \beta$.

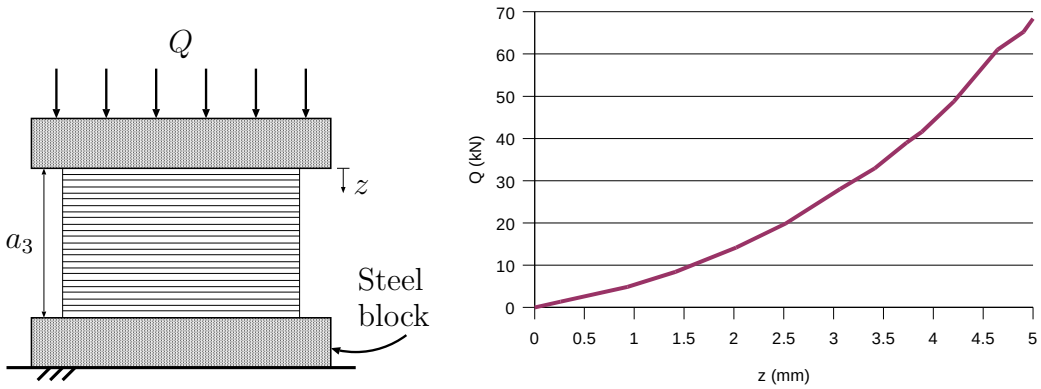

(a) Experiment (b) Response

Fig. 7. Experimental transverse load Q versus transverse displacement z. Dimensions: layer width $a_1 = 210$ mm, layer length $a_2 = 297$ mm, sample depth $a_3 = 100$ mm.

experiment that are presented in this paper primarily due to the technical difficulties encountered in the modelling of such structures that were outlined in the introduction.

A further deficiency of the earlier models is that kink banding was assumed to occur in a pressure bath; layers were held together by overburden pressure alone, and no other transverse forces, such as those that might appear from deflection into the foundation, were taken into account. As a result, once instability occurred, b could grow under constant load without limit (Hunt

et al., 2001). In the reality of the experiments this growth would be resisted by the bed of layers outside the loaded regime, an effect which appears on the scale of the multi-layered sample, not that of the individual layers. Its influence on a single layer, represented in Fig. 4(b) by the linear spring of stiffness k_f, is not easy to model from first principles, but can usefully be inferred from the experimental response of transverse load against end-shortening seen in Fig. 3, as described in §5.3.

4 Total Potential Energy Function

The elements that make up the analytical tool of the total potential energy function are next introduced in turn. A similar set of energy contributions also appear in a recent two-layer model for the related problem of *parallel folding* (Budd *et al.*, 2003). The difference between the formulations lies primarily in the assumption that all layers involved in kink banding behave identically; in parallel folding they necessarily deform to different curvatures. The governing parameters in the energy contributions are also introduced, but their experimental evaluation is covered in §5.

The formulation is taken to be volume-preserving in and around the band, in the sense that, with no movement of the transverse loading platens, no work is done with or against overburden pressure. This means that an increase in layer thickness inside the band, as described in the previous section, must be offset elsewhere by localized thinning. The only overall volume change then relates to the in-plane shortening of the springs k, which is necessary so that the system can store energy in the fundamental state.

4.1 Work done against friction

The earlier models assumed that the layers remain of constant thickness t, and took no account of spring k_f. Vertical equilibrium of an incomplete stack of blocks of Fig. 4(a) in the critical slip condition then gave the relation

$$N = \frac{qb}{1 - \mu \tan \alpha}, \tag{2}$$

where N is the compressive force between the layers in the band, and q is the overburden pressure. Note that N is only positive if $\alpha < \operatorname{arccot}(\mu)$, giving a natural limit to α where lockup occurs.

With the introduction of dilation in the band, expression (2) must be changed. As described above, we suppose that β is chosen such that $N = 0$ when $\alpha = \beta$.

Also, when the layers both in and out of the band are of equal thickness, ie in the two states $\alpha = 0$ and $\alpha = 2\beta$, we shall assume that expression (2) holds. In between these states N will be assumed to vary linearly with transverse strain. The mechanism of Fig. 6 then suggests that relation (2) should become,

$$N = \frac{qb[1 - \cos(\alpha - \beta)]}{(1 - \cos\beta)(1 - \mu\tan\alpha)}. \tag{3}$$

The pseudo-energy term U_μ, representing the work done against the friction force μN for a single layer, is then,

$$\begin{aligned} U_\mu &= \mu qb \int_0^\alpha \frac{1 - \cos(\alpha' - \beta)}{(1 - \cos\beta)(1 - \mu\tan\alpha')}\ \mathrm{d}(t\sin(\alpha' - \beta)) \\ &= \mu qbt \int_0^\alpha \frac{[1 - \cos(\alpha' - \beta)]\cos(\alpha' - \beta)}{(1 - \cos\beta)(1 - \mu\tan\alpha')}\ \mathrm{d}\alpha'. \end{aligned} \tag{4}$$

4.2 Membrane energy and work done by external load

Strain energy per layer associated with the in-line spring of stiffness k is given by

$$U_k = \frac{1}{2}k\delta^2. \tag{5}$$

The work done by the external load P acting on a single layer is simply

$$V_P = P\delta + (P - qt)b(1 - \cos\alpha). \tag{6}$$

Here the first term comes from the shortening of the in-line spring, while the second term subtracts from P a component relating to pressure q, in recognition of the volume-preserving nature of the deformation in and around the band.

4.3 Bending energy

A first estimate of the bending energy in a single layer can be obtained from a procedure described in the Appendix of Hunt *et al.* (2000), based on determining the gap between two layers undergoing identical bending deformation. An energy balance is struck between bending energy and the work done against overburden pressure in opening the gap. The formulation follows that first presented in Hunt *et al.* (2001).

For a corner of total angle α, the associated energy is obtained by minimizing

$$U_b = \frac{D}{t}\left\{\frac{1}{2}\int_{-\infty}^{\infty}\theta'(s)^2\,\mathrm{d}s + \frac{qt^3}{D}\int_{-\infty}^{\infty}f(\theta)\,\mathrm{d}s\right\},$$

where $D = Et^3/12$ is the cylindrical flexural rigidity of a layer, $f(\theta) = (k_c \sin\theta(s) + \cos\theta(s) - 1)_+$ and $k_c = \tan\alpha/2$. The minimization is done over all profiles $\theta : \mathbb{R} \to \mathbb{R}$ such that $\theta \to 0$ as $s \to -\infty$ and $\theta \to \alpha$ as $s \to \infty$. The independent variable s measures non-dimensional arc length.

It was shown in Hunt *et al.* (2000) that the minimal energy profile θ has a finite length, i.e., that there exists $s_h > 0$ such that $\theta \equiv \alpha$ if $s \geq s_h$ and $\theta \equiv 0$ if $s \leq -s_h$. With the notation $\lambda^2 = qt^3/D$, it was also shown that $s_h \sim \pi/\lambda$, approximately independently of α.

With this in mind we approximate the optimal profile by

$$\tilde{\theta}(s) = \begin{cases} 0 & s \leq -\pi/2\lambda \\ \frac{\alpha}{2}(1 + \sin\lambda s) & -\pi/2\lambda < s < \pi/2\lambda \\ \alpha & s \geq \pi/2\lambda, \end{cases} \tag{7}$$

and approximate $f(\theta)$ by $\tilde{f}(\theta) = \frac{k_c}{\alpha}\theta(\alpha - \theta)$. Thus we obtain the estimate

$$U_b \sim \sqrt{Dqt}\left\{\frac{\pi\alpha^2}{16} + \frac{\pi k_c \alpha}{8}\right\}.$$

Taking into account that $k_c = \tan\alpha/2$, we arrive at the final estimate for a single hinge,

$$U_b \sim \frac{1}{2}\, c\alpha^2 \qquad \text{with} \qquad c = \frac{\pi}{4}\sqrt{Dqt}. \tag{8}$$

4.4 Foundation energy

In Fig. 4(b), the effect of foundation resistance on a single layer is expressed by a linear spring of stiffness k_f positioned at one end of the inclined portion. The force in the spring is then

$$F_f = k_f b \sin\alpha \tag{9}$$

and the corresponding energy stored in the foundation is

$$U_f = \frac{1}{2} k_f b^2 \sin^2\alpha. \tag{10}$$

A theoretical value for the stiffness k_f can be inferred from the experimental transverse load response seen in Fig. 3, simply by altering it successively until the post-kink slope is matched. The foundation resistance can thus be dealt with in a general but quantitative way, without need to specify more precisely the actual mechanism; if we had placed the spring slightly differently, at the centre of the sample for example, the value of k_f would automatically adjust accordingly.

4.5 Nondimensionalized potential function

Addition of all energy contributions leads to the total potential energy function,

$$\begin{aligned} V &= U_\mu + U_k + U_b + U_f - V_P \\ &= \mu q b t \int_0^\alpha \frac{[1-\cos(\alpha'-\beta)]\cos(\alpha'-\beta)}{(1-\cos\beta)(1-\mu\tan\alpha')}\,\mathrm{d}\alpha' + \frac{1}{2}k\delta^2 + c\alpha^2 + \frac{1}{2}k_f b^2\sin^2\alpha \\ &\quad - P\delta - (P-qt)b(1-\cos\alpha). \end{aligned} \tag{11}$$

If the point force per layer, P, is replaced by the distributed force, $p = P/t$, the scalings,

$$V = kt^2\tilde{V}, \quad \delta = t\tilde{\delta}, \quad b = t\tilde{b}, \quad q = k\tilde{q}, \quad c = kt^2\tilde{c}, \quad k_f = k\tilde{k_f}, \quad p = k\tilde{p}, \tag{12}$$

lead to a nondimensionalized form for V:

$$\begin{aligned} V &= \mu q b \int_0^\alpha \frac{(1-\cos(\alpha'-\beta))\cos(\alpha'-\beta)}{(1-\cos\beta)(1-\mu\tan\alpha')}\,\mathrm{d}\alpha' + \frac{1}{2}\delta^2 + c\alpha^2 + \frac{1}{2}k_f b^2\sin^2\alpha \\ &\quad - p\delta - (p-q)b(1-\cos\alpha). \end{aligned} \tag{13}$$

where we have immediately dropped the tilde. From this point onwards, unless indicated otherwise, all parameters will be assumed to be in nondimensional form.

4.6 Equilibrium equations

Differentiating V with respect to the degrees of freedom δ, α and b gives the three equilibrium equations:

$$\delta - p = 0, \tag{14}$$

$$\mu q b\frac{(1-\cos(\alpha-\beta))\cos(\alpha-\beta)}{(1-\cos\beta)(1-\mu\tan\alpha)} + 2c\alpha + k_f b^2\sin\alpha\cos\alpha - (p-q)b\sin\alpha = 0, \tag{15}$$

$$\mu q\int_0^\alpha \frac{(1-\cos(\alpha'-\beta))\cos(\alpha'-\beta)}{(1-\cos\beta)(1-\mu\tan\alpha')}\,\mathrm{d}\alpha' + k_f b\sin^2\alpha - (p-q)(1-\cos\alpha) = 0, \tag{16}$$

which can readily be solved within the algebraic manipulation package Maple (Heck, 1996). The above integral is evaluated numerically within Maple us-

ing the Clenshaw–Curtis quadrature method. Fig. 8 shows some results from this computation, on plots of nondimensionalized axial load p and foundation spring force F_f against nondimensionalized total end shortening Δ, where:

$$\Delta = \delta + b(1 - \cos\alpha). \tag{17}$$

Also plotted is the relationship between p and the nondimensional band width b. Two separate solutions are obtained, the fundamental or pre-kinked solution, $\alpha = 0, p = \delta$, and the post-kink solution for which $\alpha \neq 0$. There are some noteworthy points that are appropriate here:

(1) As $\alpha \to 0$ the post-kink equilibrium path only converges to the fundamental path asymptotically implying that any linear eigenvalue analysis yields an *infinite* critical load (Hunt *et al.*, 2000).
(2) The coefficient of friction μ determines the limiting value of α calculated from eq. (2) where
$$\alpha \to \alpha_l = \operatorname{arccot}\mu. \tag{18}$$
(3) If $k_f = 0$ the axial load p tends to a constant as b increases indefinitely, as described in Hunt *et al.* (2001) and outlined in §3; if however k_f is positive, a restabilizing (positive) post-kink stiffness results and the growth in b is then limited by the appearance, under increasing load, of the next band to form.

5 Comparison with Experiments

A set of four experimental results from the rig of Fig. 1 is given in Table 1. Here Experiment 1 is that of Fig. 2, with the response shown in Fig. 3. Paper of grade 80 g/m^2 was used in each case. Direct comparison with the model requires independent estimates of k, E, q, μ and k_f, obtained in the following manner.

5.1 In-line stiffness and effective Young's modulus

The in-line stiffness k of an individual layer of thickness t and width a_1 can be determined directly from the global axial load against end-shortening response, as seen in Fig. 3, simply by dividing the initial (pre-kinked) stiffness by the number of layers. The effective Young's modulus of the paper, required for the bending stiffness estimate of equation (8), is then given by

$$E = \frac{ka_2}{ta_1}, \tag{19}$$

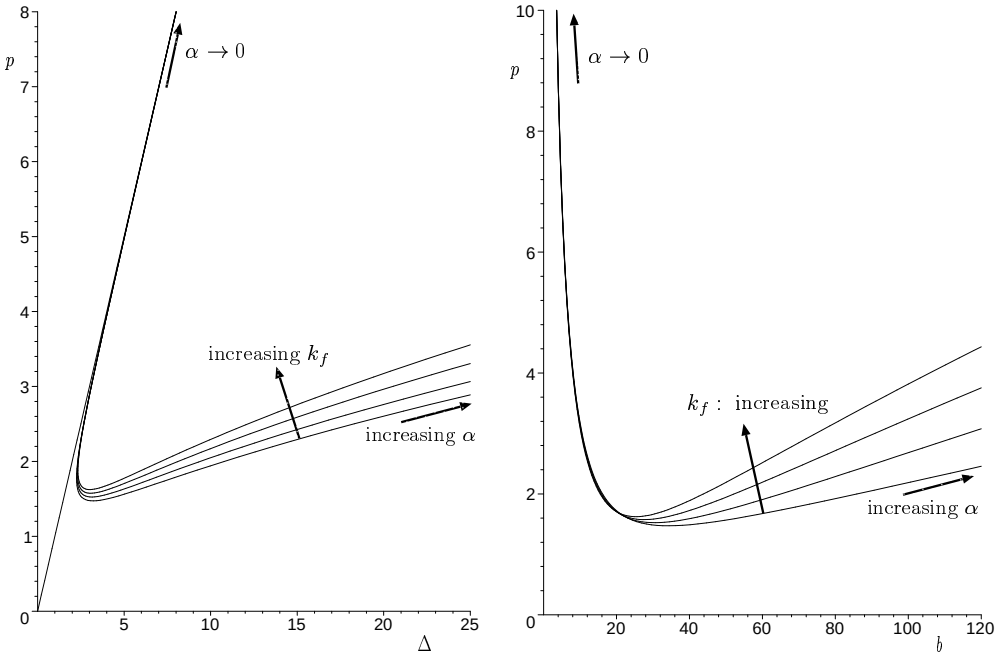

(a) Load p versus end-shortening Δ (b) Load p versus kink band width b

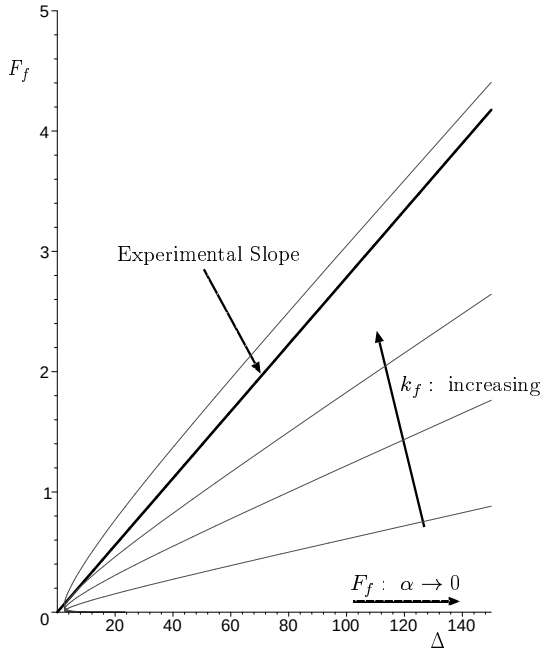

(c) Foundation force F_f versus Δ

Fig. 8. Equilibrium solutions of the model. Quantities plotted from nondimensional parameters: $q = 0.5$, $c = 10$, $\mu = 0.57$, $0.0045 \leq k_f \leq 0.0162$. Also shown is the nondimensionalized experimental slope obtained from Fig. 3.

Quantity	Experiment			
	1	2	3	4
a_1 (mm)	210	210	105	105
a_2 (mm)	297	297	297	297
a_3 (mm)	50.0	50.0	20.2	20.2
t (mm)	0.08	0.08	0.08	0.08
k (N/mm)	259.8	169.4	145.3	124.4
E (N/mm^2)	4593	2995	5139	4397
q	0.513	0.825	0.447	0.385
μ	0.57	0.57	0.57	0.57
c	9.90	12.55	9.24	8.57
k_f ($\times 10^{-2}$)	1.62	2.47	2.15	2.96

Table 1
Experimental configurations.

where a_1 and a_2 are the width and length respectively of an individual layer in the sample.

5.2 Overburden pressure and coefficient of friction

In similar manner, the nondimensional overburden pressure q can be obtained by dividing the total load Q by the length a_2 and applying the scaling of equation (12),

$$q = \frac{Q}{ka_2}. \tag{20}$$

The coefficient of friction μ of paper sliding on paper, was determined from a simple critical slope test. Layers of paper were placed on an inclined plane and the angle of inclination slowly increased until slip occurred. Simple mechanics gives the coefficient of friction as

$$\mu = \tan\gamma, \tag{21}$$

where γ is the angle of inclination at first slip. This occurred with reasonable regularity at slopes of $\gamma \approx 30^{\circ}$, so a value of $\mu = 0.57$ has been used for all comparisons.

5.3 Foundation stiffness

The foundation stiffness k_f is less straightforward to estimate. For the model, Figs 8(a) and (b) show its effect on the load/end-shortening response and the foundation spring force F_f, respectively. If the latter is taken as being solely responsible for the additional component of transverse load seen experimentally after the first kink has formed, a realistic value for k_f can be inferred by directly comparing the slopes of Fig. 3 and the dimensional form of Fig. 8(b). A procedure of successive approximation is chosen in preference to any attempt to estimate $\mathrm{d}F_f/\,\mathrm{d}\Delta$ theoretically. We do, however, make the following observation.

Fig. 8(b) indicates that the slope represented by k_f is effectively constant from an early stage in the deformation process until lockup. An estimated k_f at lockup ($\alpha = \alpha_l$) should therefore be applicable most of the range of deflection. It can be shown from equations (14)–(16) that b, δ, $\mathrm{d}b/\,\mathrm{d}\alpha$ and $\mathrm{d}\delta/\,\mathrm{d}\alpha$ all approach infinity as $\alpha \to \alpha_l = \operatorname{arccot}\mu$. If b and δ reach this limiting value more slowly than their corresponding derivatives, then it can be shown that the following relation holds in the limit:

$$\frac{\mathrm{d}F_f}{\mathrm{d}\Delta} = k_f \left(\frac{\sin\alpha_l}{1-\cos\alpha_l} \right). \tag{22}$$

This certainly is true for all cases considered here and we suspect it always to be the case, although we have no general proof.

5.4 Final comparisons

This section presents direct comparisons between the experimental results for the configurations of Table 1, and the suitably-dimensioned solutions of equations (14)–(16). The raw experimental output of axial and transverse loads versus end-displacement Δ was seen in Fig. 3 for the illustrative case of Experiment 1; similar output for the remaining three experiments is given in Fig. 9.

The experimental load–displacement curves plotted against their theoretical counterparts, and plots of kink band width b versus Δ, are shown in Figs. 10–11. Comparisons are also presented in Table 2 of the minimum post-kink experimental load level $P_{\min}$, which is the load at the experiment's restabilization point, and kink band width b_c at the applied displacement shown as Δ_c; the latter will be close to, but not necessarily at, the position of minimum experimental load, the one second time interval in the logging sequence introducing a small element of uncertainty. The comparisons are very encouraging.

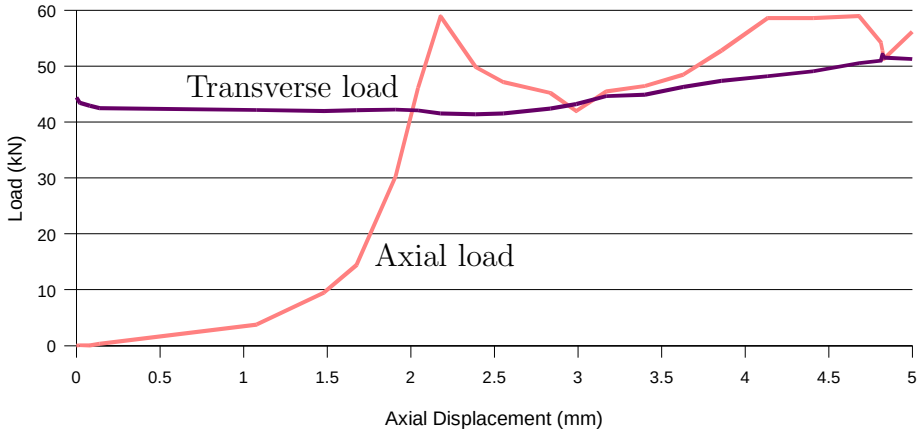

(a) Experiment 2

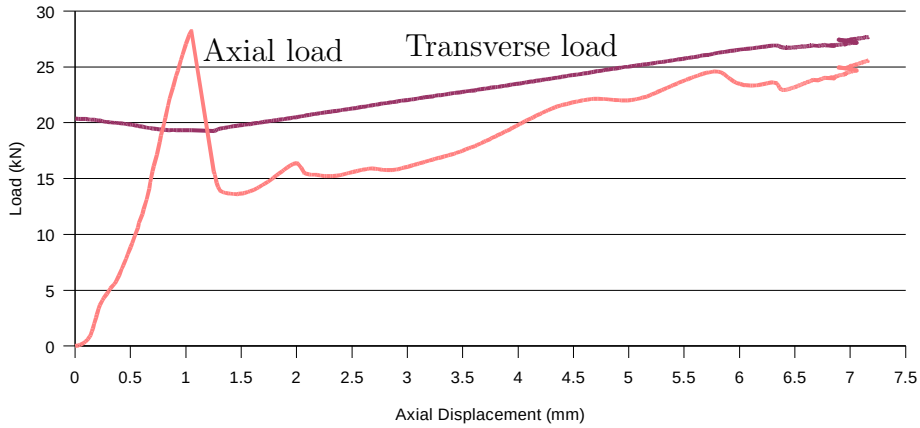

(b) Experiment 3

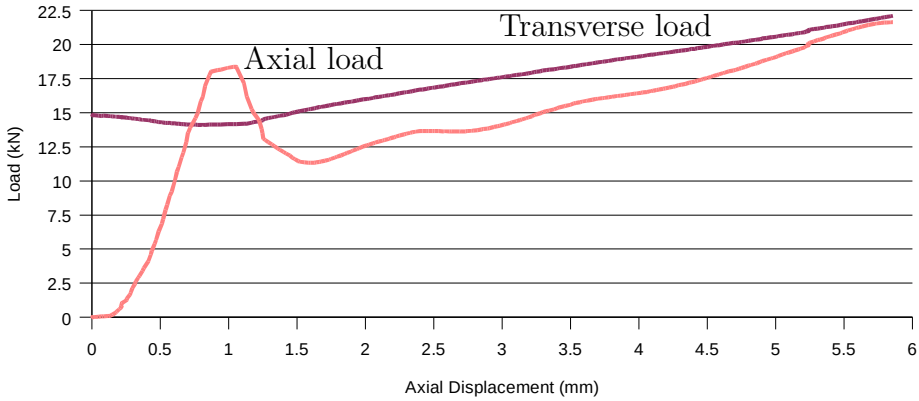

(c) Experiment 4

Fig. 9. Axial and transverse loads (P and Q) plotted against end-displacement Δ for the remaining three experiments of Table 1.

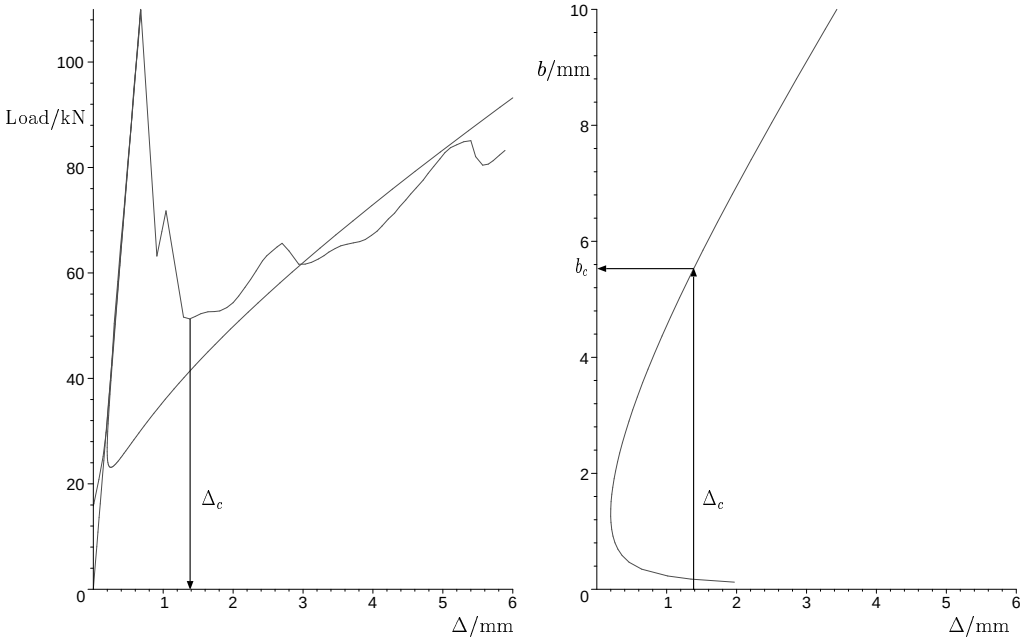

(a) Experiment 1

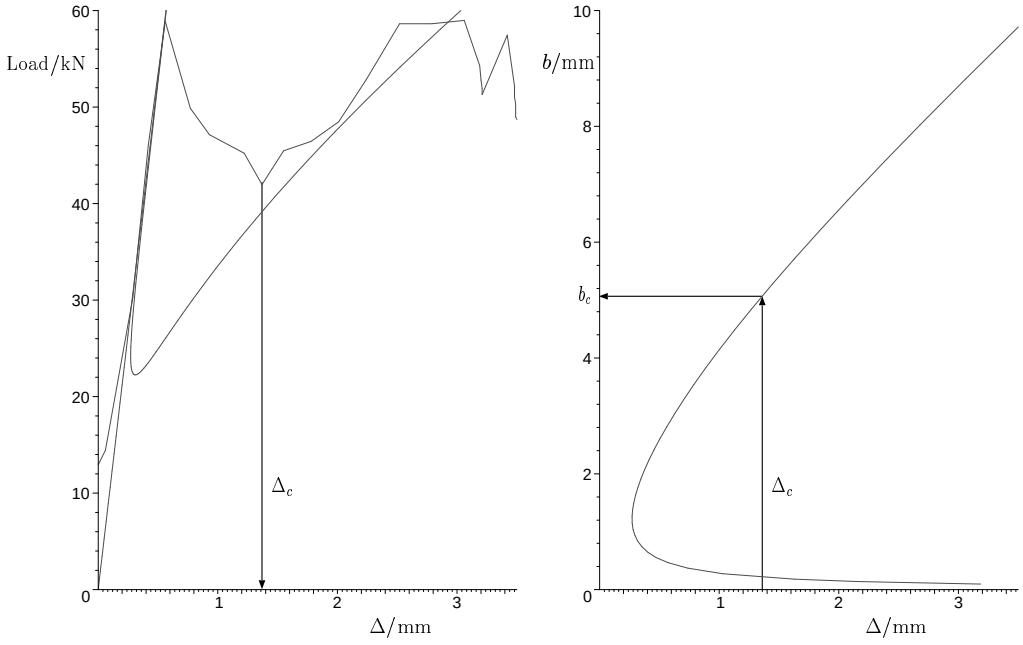

(b) Experiment 2

Fig. 10. Experiments 1–2: Load and band width comparison with end-shortening.

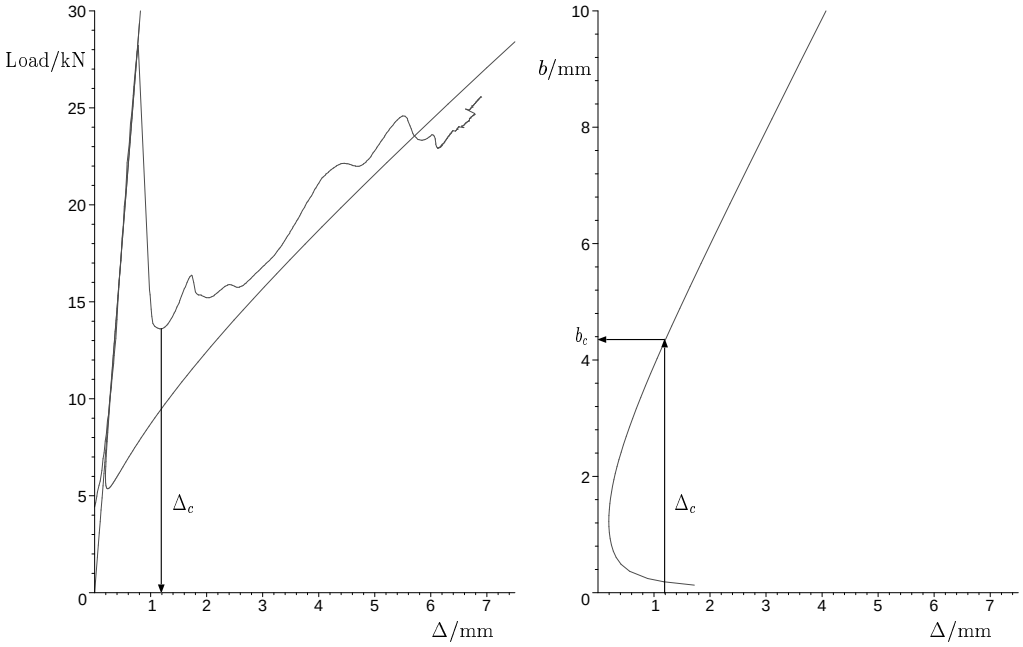

(a) Experiment 3

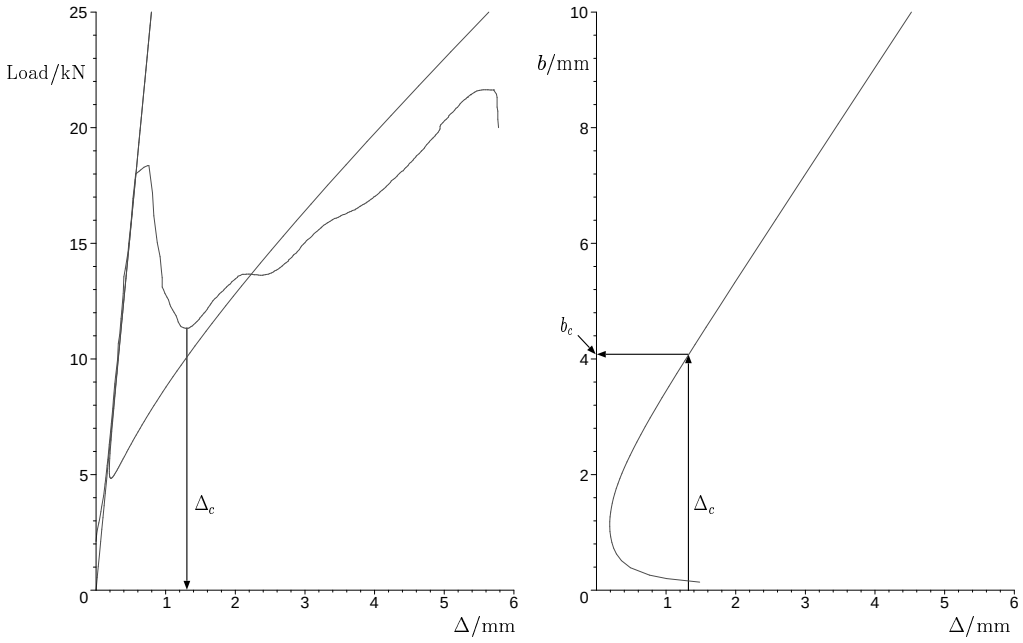

(b) Experiment 4

Fig. 11. Experiments 3–4: Load and band width comparison with end-shortening.

Expt	Theoretical values			Experimental values				% difference		
	β (deg)	Load (kN)	b_c (mm)	β (deg)	$P_{\max}$ (kN)	$P_{\min}$ (kN)	b (mm)	β	Load	b (range)
1	15.8	41.5	5.5	18.0	109.9	51.3	4.5–5.6	13.9	23.6	$-18.2 \rightarrow +1.8$
2	16.0	39.1	5.1	18.0	59.0	42.0	4.9–5.5	12.5	7.4	$-3.9 \rightarrow +7.8$
3	15.6	9.54	4.3	15.0	28.2	13.6	4.1–4.7	3.8	42.6	$-4.7 \rightarrow +9.3$
4	14.2	10.1	4.1	14.0	18.4	11.3	3.5–5.5	1.4	11.9	$-14.6 \rightarrow +34.1$

Table 2
Experimental values of kink band orientation angle β, width b_c and load levels at the initial instability $P_{\max}$ and the point of restabilization $P_{\min} = P(\Delta_c)$ compared against the model predictions at the point of restabilization ($\Delta = \Delta_c$).

The theoretical model has an infinite critical load, so no comparison is possible for the initial point of instability. However the load–displacement curves in Figs. 10–11 show good agreement between experiment and theory, both at the point of restabilization and in the subsequent slope of the post-kink response. The experimental values of β in Table 2 are given for the first band to form; subsequent bands formed at slightly higher angles of orientation, presumably as a result of the increase in transverse load with continuing propagation.

The variation of kink band widths in the experimental sample arose as the bands propagated under continued applied end-displacement; the newer bands tended to have progressively smaller widths because the lateral load Q was increasing. Moreover, under further end-displacement the bands, which initially broadened rapidly from having effectively zero width with straight edges, reached lock-up and their edges slowly began to ovalize—see Fig. 12 for an appropriate photograph of Experiment 3. As expected, the photograph also shows that the freshly formed bands have straight edges (leftmost band shown in Fig. 12). This band edge ovalization phenomenon alongside band broadening are key physical processes that eventually lead to the formation of chevron folds in stratified rock structures; the combination of these processes leads to adjacent bands merging together to form chevrons. However, this process from kink bands to chevrons usually also requires some reduction in the confining pressure.

6 Concluding Remarks

The comparisons between the experiments and the theory demonstrate that good agreement can be achieved from this simple mechanical model, provided certain important characteristics are included, viz:

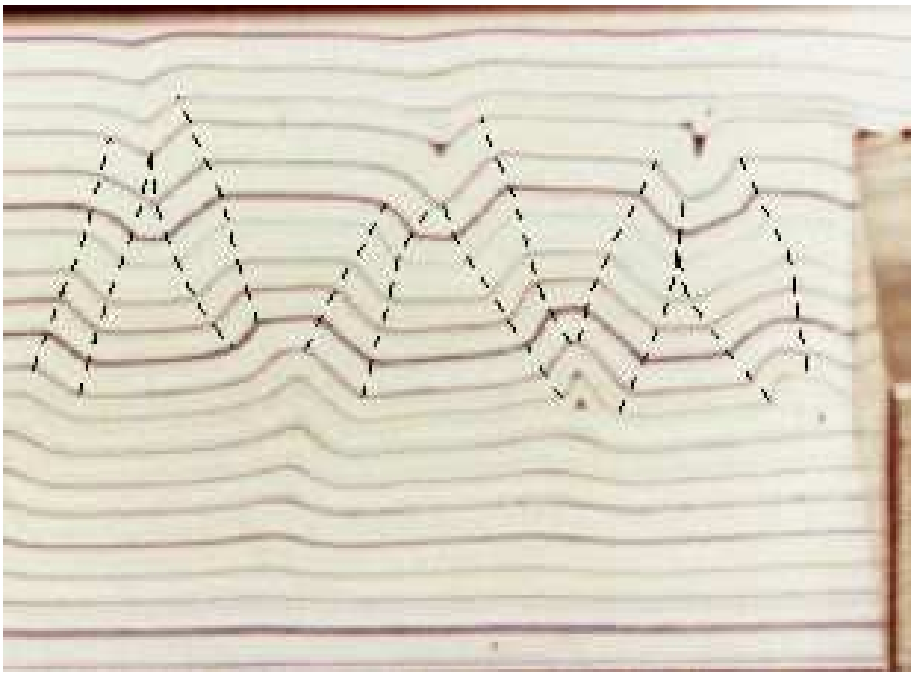

Fig. 12. Experiment 3: Finally deformed experimental sample with dashed lines superimposed to emphasize the shape of the edge of the kink bands. The first band in the loading sequence appeared on the right. Note the increasingly ovalized nature of the band edges from left to right.

(1) Bending energy: as with models of the continuous strut on elastic foundation (Hunt *et al.*, 1989; Budd *et al.*, 2003), a balance between bending energy and other energy contributions (quasi-friction and/or foundation energy terms) sets a length scale to the buckle pattern (here band width b). Bending energy was omitted in an earlier formulation (Hunt *et al.*, 2000), so b needed to be fixed a priori.
(2) Transverse compressibility of layers: optimum dilation within the band determines the kink band orientation β at the point of instability. This is then fixed for the subsequent loading history.
(3) Foundation energy: this adds a nonlinear (stiffening) resistance with respect to growth of band width. It forces the system to restabilize and ultimately limits the growth of b.

We see that good agreement is reached in terms of load levels, band orientation, band width and post-kink stiffness. Moreover the model inherently allows for the two propagation mechanisms of band broadening (growth in b) and band progression (restabilization and formation of further bands), each type having been observed during the course of the experiments. Higher order effects such as those associated with non-Coulomb friction models and band edge ovalization are perhaps avenues for developing the current model in the future.

In a number of publications found in the fibre composite literature, (for example, Budiansky (1983) and Kyriakides *et al* (2001)) it is either stated or implied that band orientation is notoriously hard to predict. Here a simple modelling concept (optimum dilation/pressure release within the band) leads to predictions which differ from those obtained experimentally by only 1 or 2 degrees. Although it is interesting to speculate that a similar mechanism may be in operation for the case of fibres within an enveloping matrix, we leave the detailed development of such an argument to future work.

Finally we note that, except for the reorientation of the layers, the stress state within the band is sometimes taken as being the same as that outside (Johnson, 1995). Our earlier constant thickness models (Hunt *et al.*, 2000; Hunt *et al.*, 2001) did reflect this assumption, but in the present model it is most definitely not the case. The dilation in the banded region leads to a drop in normal reaction between the layers, and orientates the band such that friction is minimised. As total volume is maintained over the instability, this indicates an arching of compressive stress around the band; stresses within the band are reduced, while those just outside are increased. The combined effect leads to a linear growth in the total transverse load over multiple band formation, as seen experimentally.

Acknowledgement

The authors would like to thank Ron Millward of the Structures Laboratory in the Department of Civil and Environmental Engineering at Imperial College London for constructing and helping to develop the testing rig. This work has been supported by the UK Engineering and Physical Sciences Research Council (EPSRC) through grant GR/R37173.

References

Anderson, T. B. 1964. Kink-bands and related geological structures. *Nature*, **202**, 272–274.

Argon, A. S. 1972. Fracture of composites. *Treatise Mater. Sci. Technol.*, **1**, 79–114.

Budd, C. J., Edmunds, R., & Hunt, G. W. 2003. A nonlinear model for parallel folding with friction. *Proc. R. Soc. Lond.*, A. In press.

Budiansky, B. 1983. Micromechanics. *Comput. & Struct.*, **16**, 3–12.

Budiansky, B., Fleck, N. A., & Amazigo, J. C. 1998. On kink-band propagation in fiber composites. *J. Mech. Phys. Solids*, **46**, 1637–1653.

Byskov, E., Christoffersen, J., Christensen, C. D., & Poulsen, J. S. 2002.

Kinkband formation in wood and fiber composites—morphology and analysis. *Int. J. Solids Struct.*, **39**, 3649–3673.

Fleck, N. A. 1997. Compressive failure of fiber composites. *Adv. Appl. Mech.*, **33**, 43–117.

Ghosh, S. K. 1968. Experiments of buckling of multilayers which permit interlayer gliding. *Tectonophysics*, **6**, 207–249.

Heck, A. 1996. *Introduction to Maple*. New York: Springer.

Hobbs, B. E., Means, W. D., & Williams, P. F. 1976. *An outline of structural geology*. New York: Wiley.

Hobbs, R. E., Overington, M. S., Hearle, J. W. S., & Banfield, S. J. 2000. Buckling of fibres and yarns within ropes and other fibre assemblies. *J. Textile Inst.*, **91**(3), 335–358.

Hull, D., & Clyne, T. W. 1996. *An introduction to composite materials*. 2nd edn. Cambridge Solid State Science Series. Cambridge University Press.

Hunt, G. W., Bolt, H. M., & Thompson, J. M. T. 1989. Structural localization phenomena and the dynamical phase-space analogy. *Proc. R. Soc. Lond.*, A **425**, 245–267.

Hunt, G. W., Peletier, M. A., & Wadee, M. Ahmer. 2000. The Maxwell stability criterion in pseudo-energy models of kink banding. *J. Struct. Geol.*, **22**(5), 667–679.

Hunt, G. W., Wadee, M. Ahmer, & Peletier, M. A. 2001. Friction models of kink-banding in compressed layered structures. *In:* Mühlhaus, H.-B., Dyskin, A. V., & Pasternak, E. (eds), *Proceedings of the international workshop on bifurcation and localisation in geomechanics 1999*. Lisse: Swets & Zeitlinger.

Johnson, A. M. 1995. Orientations of faults determined by premonditory shear zones. *Tectonophysics*, **247**, 161–238.

Kyriakides, S., Arseculeratine, R., Perry, E. J., & Liechti, K. M. 1995. On the compressive failure of fiber reinforced composites. *Int. J. Solids Struct.*, **32**, 689–738.

Price, N. J., & Cosgrove, J. W. 1990. *Analysis of geological structures*. Cambridge University Press.

Reid, S. R., & Peng, C. 1997. Dynamic uniaxial crushing of wood. *Int. J. Impact Eng.*, **19**, 531–570.

Rosen, B. W. 1965. Mechanics of composite strengthening. *Chap. 3, pages 37–75 of:* Bush, S. H. (ed), *Fiber composite materials*. American Society of Metals.

Vogler, T.J., & Kyriakides, S. 2001. On the initiation and growth of kink bands in fiber composites. Part I: experiments. *Int. J. Solids Struct.*, **38**, 2639–2651.

Vogler, T.J., Hsu, S.-Y., & Kyriakides, S. 2001. On the initiation and growth of kink bands in fiber composites. Part II: analysis. *Int. J. Solids Struct.*, **38**, 2653–2682.